Biomass Conversion and Biorefinery
https://doi.org/10.1007/s13399-020-00925-5

ORIGINAL ARTICLE

Effect of preparation method and B-side metal type on the physicochemical properties of $LaBO_3$ perovskite catalyst and its catalytic behaviour in the biomass pyrolysis

Nurgül Özbay [1,2] · Rahmiye Zerrin Yarbay Şahin [1,2]

Received: 21 May 2020 / Revised: 21 July 2020 / Accepted: 23 July 2020

Abstract
Although perovskites are extensively investigated in many areas, studies using perovskites as catalysts for biomass pyrolysis are still quite limited. While various transition metals can be inserted into perovskites to form different perovskites, it is critical to investigate the effects of various transition metallic substituents on the characterization of catalysts. This work involves the evaluation of nine perovskite-type catalysts in terms of their effectiveness and suitability for pyrolysis of date stone biomass. $LaCoO_3$, $LaMnO_3$ and $LaNiO_3$ perovskite catalysts were prepared by sol-gel, hydrothermal and microwave methods and characterized by X-ray powder diffraction, scanning electron microscopy and surface area measurement. Pyrolysis of date stones has been performed in tubular reactor at 520 °C with 100 °C/min and a nitrogen gas flow rate of 100 cm^3/min. The influences of catalyst preparation method on catalytic cracking of pyrolysis vapours in terms of bio-oil yields were examined. Additionally, the effect of B metal in ABO_3 perovskite structure on catalyst character and pyrolysis yields were examined in detail. According to results, highest bio-oil yield was achieved as 23.4% with $LaMnO_3$ catalyst synthesized with sol-gel method. All perovskite-type catalysts have reduced the bio-oil yield and improved the water and gaseous yield as expected. This study paves the way for developing more challenging perovskite catalysts for the renewable energy sources.

Keywords Perovskite · Sol-gel method · Hydrothermal synthesis · Microwave synthesis · Catalytic pyrolysis · Catalyst effectiveness

1 Introduction

Renewable biomass-based liquid fuels have advantages like being CO_2 neutral, being simple to transport and having low sulphur content compared with petroleum fuels which would make them primary option to fossil fuels in the future [1, 2]. One of the promising techniques to produce liquid fuels as of biomass is known as pyrolysis. It is one of the best methods for proficient conversion of feedstock into valuable products. The operation takes places in an inert ambience (1 bar, N_2) and at fair temperature (400–550 °C) within short residence time. Lignocellulosic structured biomass pyrolysis is graded in three products; liquid (bio-oil), solid (bio-char) and gas. Low-quality and dark brown bio-oils cannot be utilized in diesel engines because they are quite unstable as being oxygenated. Therefore, the bio-oil requires to be upgraded to eliminate its oxygenated compound contents in terms of high acidity, viscosity and water contents [1].

Catalytic pyrolysis is generally utilized for bio-oil upgrading and tar reforming/wax elimination. It involves the adding of catalysts to the pyrolysis. Using the catalyst can develop the products' quality and leads to the selection of valuable products. The catalyst's usage is supposed to improve the reactions of the tar molecules in pyrolysis products giving lighter and less complex tar molecules [3, 4]. The catalysts enhance the quality of the pyrolysis bio-oil through cracking, deoxygenation, oligomerization, cyclization, aromatization, alkylation, isomerization and polymerization [5]. In particular, deoxygenation proceeds from by three main pathways; decarboxylation, decarbonylation and dehydration producing CO_2, CO and H_2O, respectively [6]. The catalysts are

✉ Nurgül Özbay
nurgul.ozbay@bilecik.edu.tr

[1] Chemical Engineering Department Faculty of Engineering, Bilecik Seyh Edebali University Gulumbe Campus, 11230 Bilecik, Turkey

[2] Biotechnology Application and Research Centre, Bilecik Şeyh Edebali University, 11230 Bilecik, Turkey

Published online: 07 August 2020

also noticed as decreasing the formation of carboxylic acids which makes bio-oil less corrosive and persuade the reactions that take part in the removal of the reactive oxygenated species (like carbonyl compounds) making bio-oil having higher heating values and better stability [3, 7].

A high degree of deoxygenation has been accomplished using strong acidic, especially zeolitic catalysts, which generate large concentrations of aromatic hydrocarbons. However, high density of acidic sites of the catalyst leads to a sharp reduce in the bio-oil yield due to extreme cracking. Besides, the catalyst undergoes an extensive coking, which results in its rapid deactivation [6]. Developing perovskites providing a better performance in terms of bio-oil properties, such as lower oxygen content and higher quality, can help to overcome this situation.

The study of perovskites is of great interest due to the range of electrical and magnetic properties [8]. Perovskite-type materials are mixed-valence oxides with the unit formula of ABO_3. In perovskite structure, A and B are cations with coordination numbers 12 and 6, respectively, and have been extensively studied in catalytic, energy and environmental implementations. Catalytic perovskites have been examined for the reforming reactions. Furthermore, resistance to coke development and particular tolerance to sulphur poisoning of perovskite catalysts originates from a low binding energy, which appoints them appropriate for heavy-hydrocarbon reforming [9].

In the literature, there are studies in which numerous catalysts containing zeolites (like ZSM-5, HZSM-5 and FCC), alkaline (like Na_2CO_3/γ-Al_2O_3, K_2CO_3, Ca $(OH)_2$ and MgO), metal oxides (like Cu/Al_2O_3, Fe/Al_2O_3) and mesoporous catalysts (like Ni/SBA-15, Co/SBA-15, Fe/SBA-15, Al/SBA-15, Al-MCM-41) that have been utilized for bio-oil conversion [4–7, 10–12]. However, there is even less data on with perovskite catalysts in the utilization of only bio-oil upgrading systems [13, 14].

Perovskites have been rarely utilized to catalyse the conversion of biomass or its other substituents like lignin into high-value products. For instance, Wang et al. had indicated that both the conversion rate of lignin and the yield of aromatic aldehydes were enhanced when $LaFe_{1-x}Cu_xO_3$ was used to catalyse the oxidation of lignin [15]. In order to fill the lack of this area, for the first time in the literature, perovskite-type catalysts were applied on the conversion of biomass to liquid fuel without upgrading in this study.

The date tree in the world is frequently found in Middle East of Asia and Egypt, Algeria and other North African-Mediterranean countries [16–19]. As of 2004, the world's annual date production is 6.7 million tons [18, 20]. As a result of increasing demand, this number reached to 7.2 million tons in 2010. According to this production, it is accepted that approximately 720,000 tons of stone as a waste is produced annually [21, 22].

As the date stone makes up approximately 10% of the weight of the date, a considerable amount of biomass is produced annually [16, 18, 23, 24]. It is also used as a renewable energy source by direct combustion of the date core. Activated charcoal obtained from date stone is used as filter for automobile exhaust gases and adsorbent for toxic organic and inorganic compounds. There are many studies on the production of activated carbon from this agricultural waste chemical process. According to the studies, the chemical structure of the date stone with low ash content is very suitable for the production of activated carbon. Therefore, converting the date stone to activated carbon is one of the most promising and useful ways in terms of waste [18, 23, 25, 26]. It is used as a sorbent for the removal of synthetic dyes, phenol and heavy metals from the inexpensive, easy to access and renewable date stone. However, pyrolysis of the date stone is in the literature with a limited number of studies [27]. The objective of this work is to assess the catalyst performance of $LaCoO_3$, $LaMnO_3$ and $LaNiO_3$ in the pyrolysis of date stone. The effects of the catalyst preparation method, B metal type in ABO_3 perovskite structure, and bio-oil yield as desired product have been achieved. In addition, reusability of the optimum catalyst which is chosen according to bio-oil yield was studied.

2 Materials and methods

2.1 Biomass

Date stone (DS) used in this study were imported from Algeria. DS were washed with distilled water and stored at room temperature after drying. After the raw material was air-dried in the laboratory environment, it was milled in Armfield FT-7A mill. The average particle size was determined by sieving from four different sieves: $Dp > 1.8$ mm, $1.8 > Dp > 0.85$ mm, $0.85 > Dp > 0.425$ mm, and $Dp > 0.425$ mm. The proximate analysis of DS was based on the American Society for Testing and Materials (ASTM) standards (moisture content: ASTM E871–82, ash: ASTM D1102–84, volatile matter: ASTM E872–82 and fixed carbon is calculated by the difference).

2.2 Catalyst preparation

The prepared catalysts were denoted as SG, HM and MW for sol-gel method, hydrothermal synthesis and microwave method, respectively.

2.2.1 Sol-gel method

The $LaCoO_3$, $LaMnO_3$ and $LaNiO_3$ were prepared according to conventional sol-gel method [28, 29]. $La(NO_3)_3{\cdot}6H_2O$ (ABCR), $Ni(NO_3)_2{\cdot}6H_2O$ (Carlo Erba), $Co(NO_3)_3{\cdot}6H_2O$

(Carlo Erba), $Mn(NO_3)_2{\cdot}4H_2O$ (Sigma Aldrich), citric acid monohydrate $C_6H_8O_7$ (Carlo Erba) and ammonium carbonate (Carlo Erba) were utilized as reagents. Appropriate amount of the reagents was used after preparing 1 M salt solution. After adding citric acid to homogenic solution, 1 M $(NH_4)_2CO_3$ solution was added to modify pH at 6. Then, the solutions were evaporated at 60 °C to complete sol-gel formation. Drying catalysts at 210 °C in an oven was followed by calcination at 700 °C for 5 h with a heating rate of 5 °C/min.

2.2.2 Hydrothermal synthesis

The hydrothermal synthesis of $LaCoO_3$, $LaMnO_3$ and $LaNiO_3$ was carried out in 100-ml Teflon-lined reactors with a filling capacity of 50%. Before synthesis, stoichiometric amounts of $La(NO_3)_3{\cdot}6H_2O$ (ABCR), $Ni(NO_3)_2{\cdot}6H_2O$ (Carlo Erba), $Co(NO_3)_3{\cdot}6H_2O$ (Carlo Erba), $Mn(NO_3)_2{\cdot}4H_2O$ (Sigma Aldrich) solutions were prepared in advance. Then, a KOH aqueous solution was added drop by drop up to the pH value of 13 for whole co-precipitation. Crystallization was carried out in Teflon-lined reactor under autogenous pressure at 200 °C for 2 days, and finally the crystalline powder was filtered after washing with deionized water [30]. The crystalline powder was dried at 100 °C for 12 h. The final products were moved into crucible and calcined at 700 °C for 5 h with a heating rate of 5 °C/min.

2.2.3 Microwave synthesis

The precursors were prepared mixing a certain amount of nitrates of lanthanum, manganese, cobalt and nickel under stirring in the microwave synthesis procedure at room temperature. The pH was fixed at 8.5 using 1 M NH_3 solution under vigorous stirring until obtaining a homogeneous product which was then transferred into a Milestone ETHOS TC Microwave employing microwave processing [31]. The instrument which was equipped with temperature and pressure-monitoring device was operated at 200 °C and 2.45 GHz with a power supply of 720 W for 30 min. The solid products gained by centrifugation and filtration have been washed with distilled water and then dried at 100 °C for 12 h. The resulting powder was milled and then calcined at 700 °C for 5 h.

2.3 Experimental method

The pyrolysis experiments were carried out under N_2 using electricity heated and well-swept fixed-bed tubular reactor made of 310 stainless steel with a length of 90 cm and an inner diameter of 2.5 cm. Both pyrolysis temperature and heating rate were controlled using a proportional–integral–derivative (PID) controller in the tests. A rotameter was utilized to control N_2 before entering into the reactor. Temperature measurements were attained from the bed by the thermocouple in the middle of the reactor to control the temperature and were monitored from the control panel. At the end of pyrolysis, the liquid phase was collected in a glass liner located in a cold trap maintained at about 0 °C. The liquid phase involved aqueous and bio-oil phases which were divided and weighed. The solid product (char) was removed from reactor and weighed; then, the gas yield was considered by the difference.

Experiments were conducted both in the absence and presence of perovskite-type catalysts. For the first group of experiments, DS were heated up to a constant temperature of 520 °C with a constant heating rate of 100 °C/min and then held for 15 min. In the second group of tests, effects of perovskite-type catalyst preparation method and B metal in perovskite's ABO_3 structure on product yields were investigated in detail. In "in situ" catalytic pyrolysis process, a biomass sample is usually physically mixed with catalyst and pyrolysed at preferred temperature. In this work, 0.5 g catalyst was mixed with 9.5 g DS at pyrolysis temperature of 520 °C with 100 cm^3/min N_2 and heating rate 100 °C/min. All the yields were given in an ash-free and dry basis, and their values were calculated as the average of two parallel tests error less than ±0.5%.

2.4 Analytical techniques

The ultimate analysis of DS was implemented using an elemental analyser (Leco CNH628 S628) for C, H, and N. Oxygen was calculated by the difference. The thermal behaviour of DS to 1000 °C with a heating rate of 10 °C/min, under a nitrogen and air (20.8% O_2/N_2 bal.) atmosphere (50 ml/min), was studied using a Setaram, Labsys evo thermogravimetric analyser. The FT-IR spectrum of biomass was recorded using a Perkin Elmer Spectrum 100 Model in wave number range of 4000–400/cm by ATR module. The biomass and perovskite catalysts were characterized for morphologies using scanning electronic microscopy (SEM) (Zeiss Supra VP 40).

Perovskites were positioned on carbon bands and coated with a platinum thin layer in Ar atmosphere with Quorum Q150RESDC Sputter Coater. Crystalline structures of perovskites were determined via PANalytical X'Pert Pro Materials Research Diffractometer using CuKα radiation. The X-ray tube was operated at 45 kV and 40 mA and the X-ray pattern was scanned with a step size of 2°/min from 10 to 90° (2θ). The textural characteristics including Brunauer–Emmett–Teller (BET) specific area, pore volume and average pore diameter (Barrett-Joyner-Halenda (BJH) method), were measured by N_2 adsorption-desorption in a Micromeritics ASAP 2020.

2.5 Catalyst effectiveness

The performance of a catalyst depends on factors like the improved liquid product, particularly the formation of hydrocarbons containing aliphatic and aromatic compounds, the reduction of solid product and water, the acidity and pore size of the catalyst [32].

The catalyst performance is related to its activity and selectivity:

$$K_{effectiveness} = Y_i.S_i$$

In the formula, $K_{effectiveness}$ is catalyst activity, Y_i is desired product yield and S_i is desired product selectivity.

The yields are calculated using the following equations:

$$Y_i\ (w\%) = \text{desired product (g)/biomass as dry ash (g)},$$

$$S_i = \text{desired product (wt.\%)/undesired product (wt.\%)}.$$

3 Results and discussion

3.1 Biomass characterization

The proximate analysis was performed on date stones having average particle size of 1.026 mm and bulk density of 560 kg/m^3 to determine the weight fractions of moisture, volatiles, ash and fixed carbon (Table 1). DS was found richer in holocellulose (57.77%) than lignin (25.77%). Likewise, ultimate analysis was also used to determine the elemental composition by means of weight fractions of carbon, hydrogen, oxygen and nitrogen (Table 1). Using elemental analysis results, calorific value of date stone was calculated as 19.45 MJ/kg using Dulong Formula and H/C ratio was found to be 1.24. The chemical composition and higher heating value (HHV) of the DS were found in the expected range for date stone biomass, with high volatile matter contents and low ash percentages [20, 23, 24, 26].

Table 1 Proximate, structural and ultimate analyses (wt.%) of DS

Proximate analysis (%)	
Moisture	4.33
Volatile	78.85
Fixed carbon	15.86
Ash	0.97
Structural analysis (%)	
Extractives	16.46
Hemicellulose	14.81
Lignin	25.77
Cellulose (by difference)	42.96
Holocellulose	57.77
Ultimate analysis (%, dry basis)	
Carbon	54.45
Hydrogen	5.64
Nitrogen	0.53
Oxygen (by difference)	39.38
H/C	1.24
O/C	0.54
HHV (MJ/kg)*	19.45

* Calculated using Dulong formula

3.1.1 Thermal decomposition behaviour of date stone

Derivative weight loss profile of DS is illustrated in Fig. 1. In general, the pyrolysis diagram can be investigated in three parts: (i) dehydration T < 110°, (ii) devolatilization (200–600 °C), (iii) stabilization and decomposition of the carbonaceous matter (600–800 °C) [33]. According to thermal gravimetric (TG) and thermogravimetric derivative (DTG) curves of DS, first weight loss occurred in the range of 80–225 °C with the removal of the moisture. This weight loss, which indicates the amount of moisture contained in the biomass, is 5.36%. The main decomposition of the DS arose in the temperature range between 200 and 500 °C. The sharp peak at 233 °C is ascribed as hemicellulose and a second sharp peak at 344 °C indicates the cellulose. Lignin decomposition occurred between 200 and 700 °C. The matter remaining after the mass losses in the biomass comes from the ash and undecayed carbon.

3.1.2 FT-IR spectrum of date stone

FT-IR spectra were taken to elucidate the chemical structure of the raw material and the analysis result is given in Fig. 2. In the figure, it is obvious that the date stone consists of various functional groups. When the spectrum is examined, the wide and widespread -OH peaks observed at 3309–3295 cm^{-1} indicate the presence of alcohol, phenol or carboxylic acids; 2922–2853 cm^{-1} in the peak seen asymmetric and symmetrical C-H vibrations show the presence of aliphatic structures. The peaks around 1743–1740 cm^{-1} represent carbonyl groups, while the peaks between 1634 and 1615 cm^{-1} originate from olefinic C=C vibrations and C=O vibrations found in aromatic structures. The peaks observed around 1029–1016 cm^{-1} are due to C-O vibrations. Peaks showing aromatic C-H structure in the range of 918 cm^{-1} and 717 cm^{-1} were observed.

3.1.3 SEM images of date stone

SEM is a potential technique for exploring morphology of solid fuel particles [34]. When the SEM images in Fig. 3 were examined, the date stone has indented protruding particles and an almost non-porous structure. Date stone has some internal

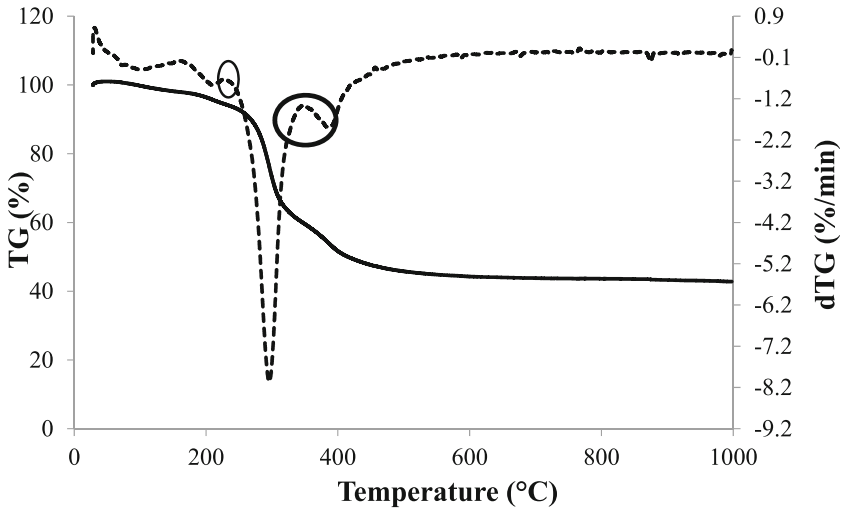

Fig. 1 Derivative weight loss profile of DS

pores and cracks, while obvious pores not distinctively found. Date stone particles have irregular shapes in deed.

3.2 Characteristics of prepared catalysts

Catalysts prepared by sol-gel, hydrothermal and microwave methods were denoted as SG, HM and MW, respectively. Cobalt, manganese and nickel were labelled as Co, Mn and Ni, respectively.

3.2.1 Specific surface area (S_{BET})

One of the major problems related to perovskite synthesis is lower specific surface area achievement when compared with other metal oxides [35]. The results of the BET specific surface area (S_{BET}) of the synthesized catalysts are illustrated in Fig. 4. The Mn-based samples calcined at 700 °C have comparatively higher S_{BET} values which are approximately 10.3 m^2/g. Conversely, S_{BET} values of Ni-based and Co-based catalysts are ca. 7.9 and 6.8 m^2/g, respectively. While the highest surface area catalysts for $LaMnO_3$ and $LaNiO_3$ were obtained by microwave method, the highest surface area of $LaCoO_3$ catalyst was found in hydrothermal method. Generally, sol-gel method leads to lower surface area when compared with the other methods.

S_{BET} results are quite in agreement with the results of the $LaCoO_3$, $LaMnO_3$ and $LaNiO_3$ catalysts found in the literature [28, 36, 37]. As a result, it was observed that there is an apparent effect on the surface area of the preparation method when compared to B metal selection.

3.2.2 X-ray diffraction (XRD)

Figure 5 shows the ex-situ XRD profiles of $LaCoO_3$, $LaMnO_3$ and $LaNiO_3$ catalysts. XRD patterns prove the presence of the perovskite characteristic diffraction lines at 32.84°, 32.56° and 32.77° for sol-gel synthesized $LaCoO_3$ (ref. code: 98-015-6452), $LaMnO_3$ (ref. code: 98-009-6038) and $LaNiO_3$ (ref. code: 98-009-1042), respectively. In $LaCoO_3$ samples, cubic Co_3O_4 (ref. code: 98-062-4571) was observed to be formed

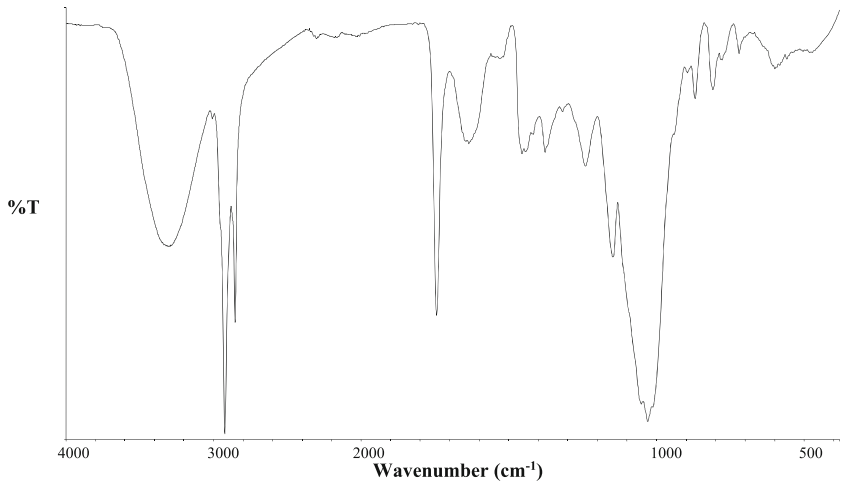

Fig. 2 FT-IR spectrum of date stone

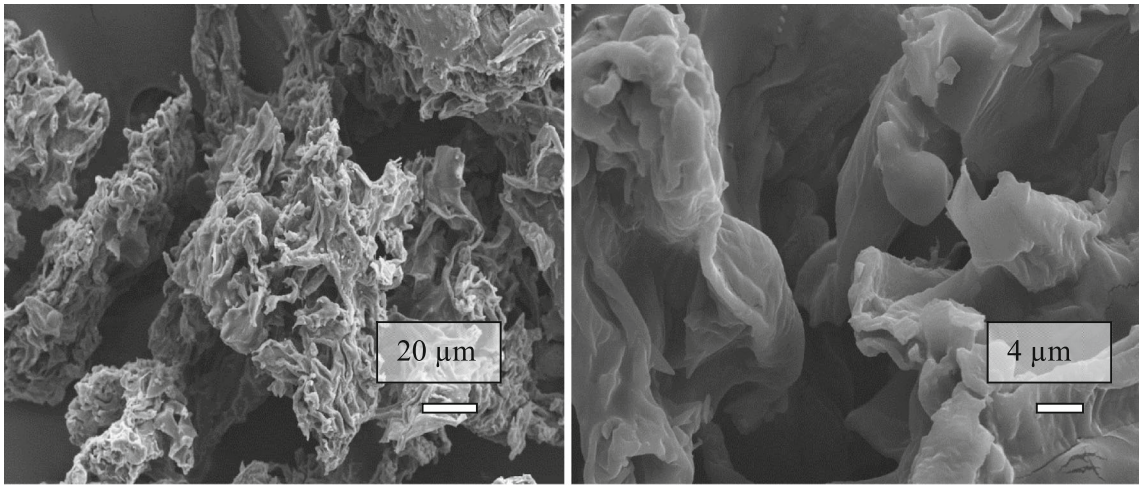

Fig. 3 Date stone micrographs

during the thermolysis of the citrato complex and it has not entered the composition of the cobaltate with very low peak intensity obtained by applying sol-gel method [38]. On the other hand, orthorhombic $La_4Co_3O_{10}$ (ref. code: 98-008-6177) and hexagonal H_3LaO_3 (ref. code: 98-024-5674) phases were observed in the hydrothermally prepared catalyst. In the XRD spectrum of the catalyst prepared by microwave method, orthorhombic $La_4Co_3O_{10}$ (ref. code: 98-008-6177) and cubic Co_3O_4 (ref. code: 98–062-4571) phases are observed. In the literature, $La_4Co_3O_{10}$ phase has been detected in solid-state synthesis when the cations were not in good proportions. Besides, the lack of lanthanum or the excess of cobalt are known to partially stabilize the $La_4Co_3O_{10}$ phase, remaining at ambient temperature [39].

Hexagonal $LaMnO_3$ (ref. code: 98-009-0355) and hexagonal La_2O_3 (ref. code: 98-004-4692) phase have been observed in hydrothermal method in trace amount at $2\Theta = 48.7°$. It is believed that the different (or assumed as impurity in the literature) phases formed are caused by the fact that lanthanum migrates to different forms in dry air atmosphere during calcinations. The monoclinic $LaMnO_3$ (ref. code: 98-016-2003) and hexagonal H_3LaO_3 (ref. code: 98-024-5671) phases were formed in the XRD spectrum of the catalyst prepared by the microwave method.

XRD plots of $LaNiO_3$ catalysts illustrated that hexagonal $LaNiO_3$ (ref. code: 98-009-1042) phase and orthorhombic La_2NiO_4 (ref. code: 98-006-3398) were obtained by sol-gel method. The XRD graph of the hydrothermally prepared $LaNiO_3$ catalyst shows that the structure consists of hexagonal $LaNiO_3$ and a small amount of hexagonal La_2O_3 (ref. code: 98-010-0205) phases at $2\Theta = 43.4°$. Only the tetragonal La_2NiO_4 (ref. code: 98-000-2569) is visible in the XRD spectrum of the catalyst prepared by the microwave method. The structure of La_2NiO_4 seen in microwave method belongs to the perovskite structure of A_2BO_4 [40, 41]. Previous studies have shown that at low calcination temperatures, the amount of pure perovskite is insufficient, while pure perovskite is obtained at 850 °C. However, the amount of La_2NiO_4 phase

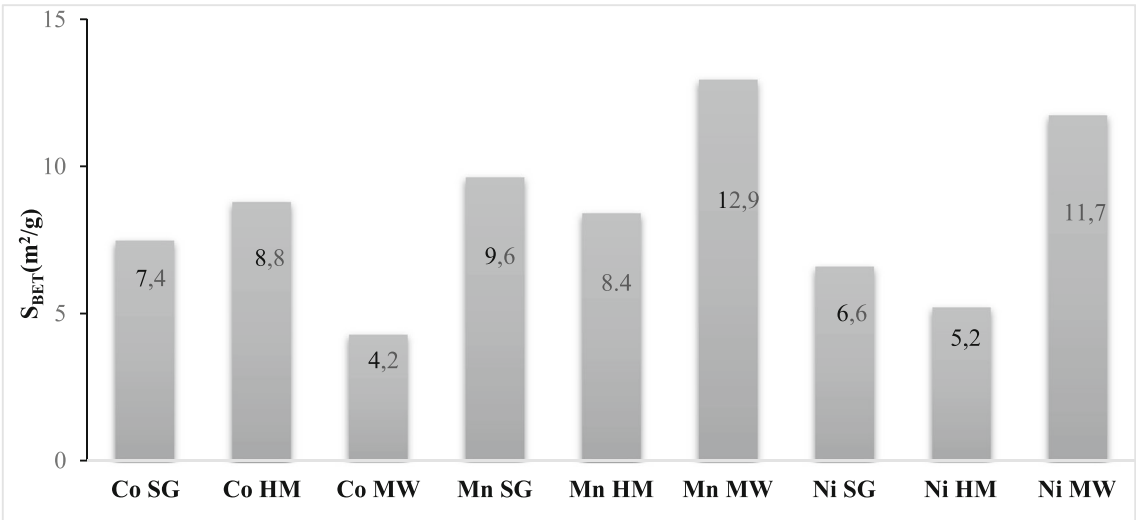

Fig. 4 S_{BET} results of the perovskite catalysts

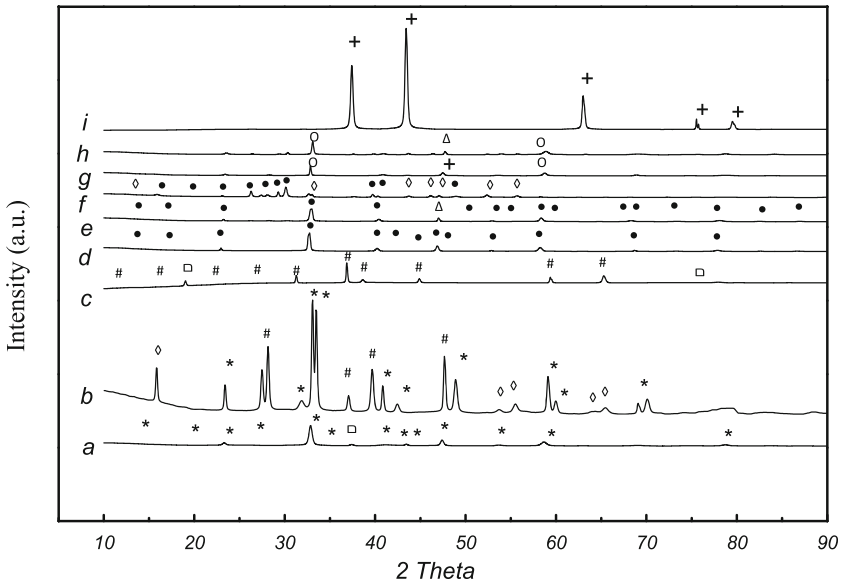

Fig. 5 XRD patterns of **a** Co SG, **b** Co HM, **c** Co MW, **d** Mn SG, **e** Mn HM, **f** Mn MW, **g** Ni SG, **h**Ni HM, and **i** Ni MW perovskite catalysts. * $LaCoO_3$, ● $LaMnO_3$, O $LaNiO_3$, ◊ H_3LaO_3, Δ La_2O_3, Co_3O_4, # $La_4O_3O_{10}$, + La_2NiO_4

increased as Ni migrated to Ni^{+2} form at higher temperatures [40].

Among the synthesis methods, sol-gel was found to be superior when pure phase is considered. Different perovskite structures can be accomplished via microwave method.

The pore size distributions of the catalysts in terms of Harkins and Jura [42] plot with FAAS correction are given in Fig. 6. The pores in structures of perovskites were well and not uniformly distributed. Wide pore size distribution for the whole samples was observed, ranging from 5 to 80 nm. The BJH cumulative pore volume curves given in Fig. 6 also indicate the loss in pore volume in case of cobalt used perovskites. Figure 6 indicates that the decrease in pore volume is more important in the micropore region. For better comparison, the volume in the entire range of pores is divided into two regions which were corresponded to the pores of diameters up to 50 and 50–100 nm, respectively. Thus, using different metals affects in terms of more volume in micropores and smaller mesopores (up to 50 nm) compared with that of the larger mesopores (> 50 nm) and macropores (> 125 nm).

3.2.3 Scanning electron microscopy

SEM images of $LaCoO_3$, $LaMnO_3$ and $LaNiO_3$ are shown in Fig. 7 with different magnification sizes. When SEM images of catalysts prepared by different methods are examined, the sol-gel-prepared catalysts (Fig. 7a, d, g) are found as spongy-like structures and contain small pores. These pores can be described as gas outlet points and are assumed to be at the temperature at which the catalyst produces intense NO_x gas between 120 and 220 °C during the drying gel stage. SEM images of the catalysts prepared by hydrothermal synthesis (Fig. 7b, e, h) showed spherical particles bringing pores. The particles are seen in clustered groups. In the $LaCoO_3$ catalyst synthesized by the hydrothermal method, rod clusters occasionally occurred. In microwave synthesis, the target which is small particle in size has been attained. While $LaNiO_3$ composition displayed small spherical particles, microwave synthesis had led the $LaMnO_3$ catalyst obtain large spherical particles and clustered and occasionally rod-like structures. When the catalysts were prepared by microwave method (Fig. 7c, f, i), quick crystallization occurred compared with hydrothermal method as expected. Besides, this quick crystallization leads formation of agglomeration in some parts of $LaMnO_3$ catalyst.

3.3 Catalytic activity

In this study, non-catalytic and catalytic date stone pyrolysis was evaluated in terms of product yields. Indeed, the catalytic pyrolysis experiments investigated the influence of (a) the catalyst preparation method and (b) the nature of B metal on activity.

As a result of the non-catalytic pyrolysis experiments (Fig. 8), the yield of bio-oil was found to be 24%. In case of catalyst existence, the catalyst preparation method and active metal side (B) affected the surface properties, morphology, homogeneity and particle size of the catalyst as mentioned in the literature [43]. All these factors directly affected the product yields. Among the three methods used, the highest bio-oil yields were obtained by the sol-gel method which were followed by microwave and hydrothermal methods. When active metal side effects are compared, the highest bio-oil yield was obtained with the manganese metal used ones for all synthesis methods.

In the presence of catalyst in pyrolysis, bio-oil, char and gas yields decreased. The decrease for the bio-oil when a perovskite catalyst used could be attributed to competing reaction,

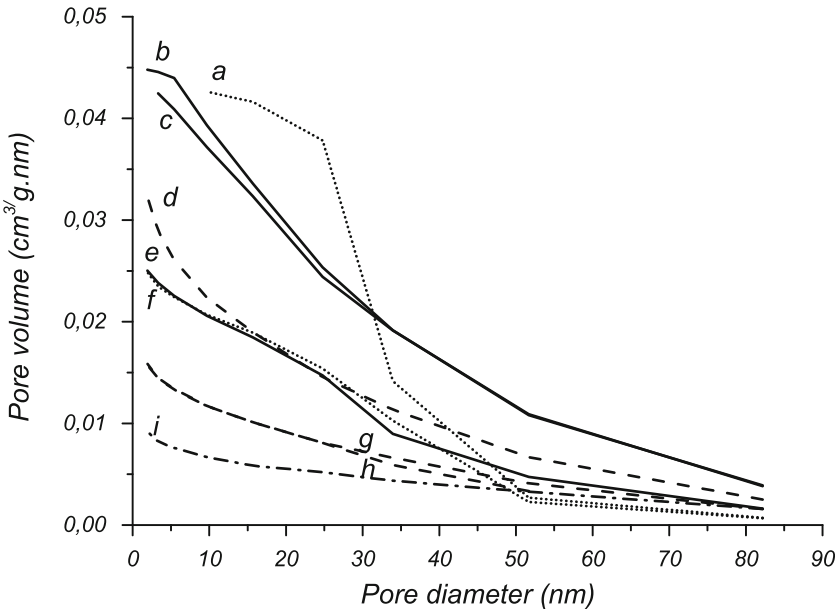

Fig. 6 The pore size distribution of **a** Ni SG, **b** Mn MW, **c** Mn SG, **d** Ni MW, **e** Co HM, **f** Mn HM, **g** Co SG, **h** Ni HM, and **i** Co MW perovskites

most likely conversion reactions occurring during pyrolysis. This suggests that the additional conversion of bio-oils over the catalysts resulted in a decrease of bio-oil yield. Besides, the perovskite catalysts helped conversion of the biomass oxygen to water and thus resulting in low liquid yield. The incorporation of the perovskite to the reaction system caused to

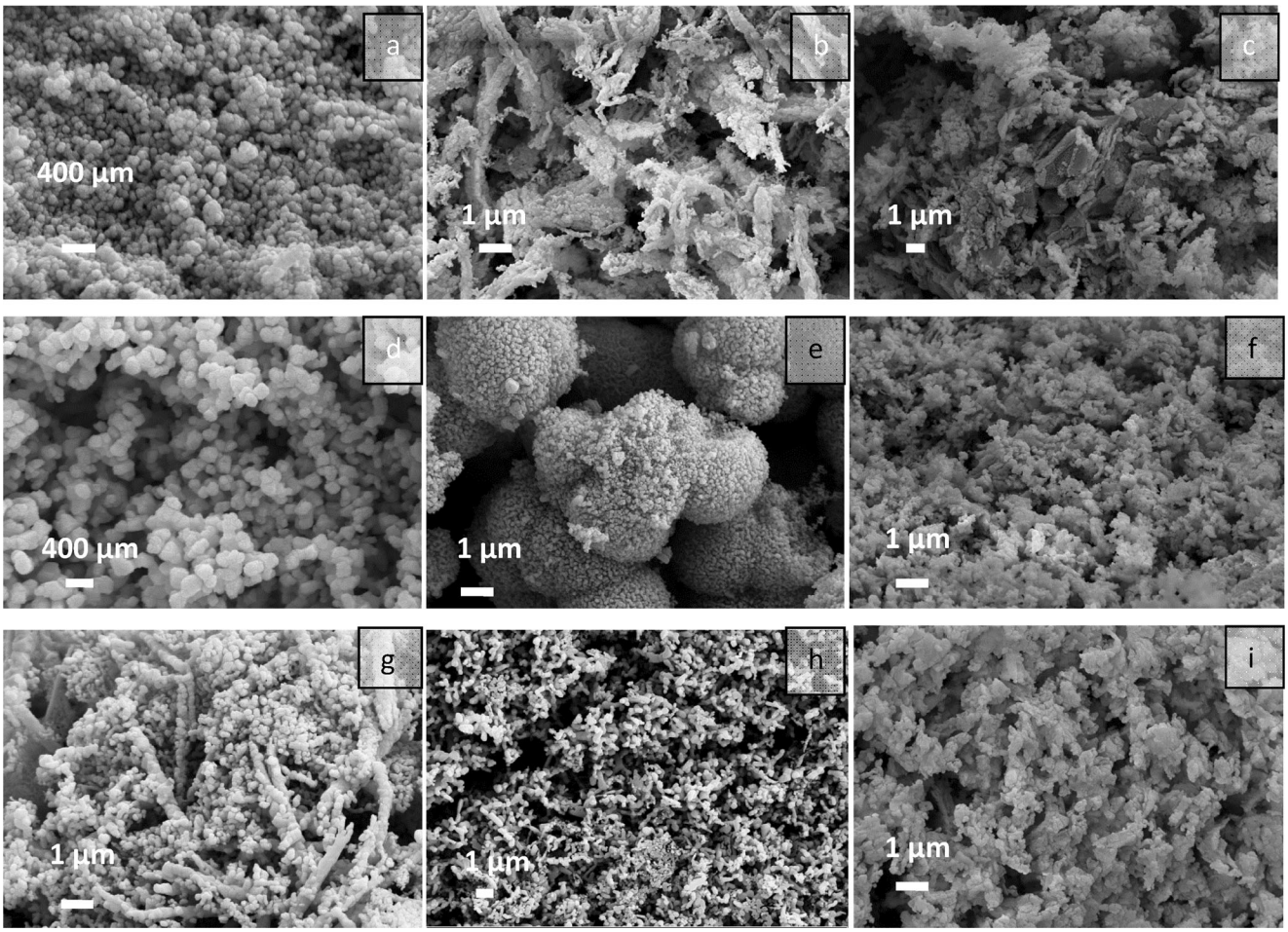

Fig. 7 SEM images of the perovskite catalysts **a** Mn SG, **b** Mn HM, **c** Mn MW, **d** Ni SG, **e** Ni HM, **f** Ni MW, **g** Co SG, **h** Co HM, **i** Co MW

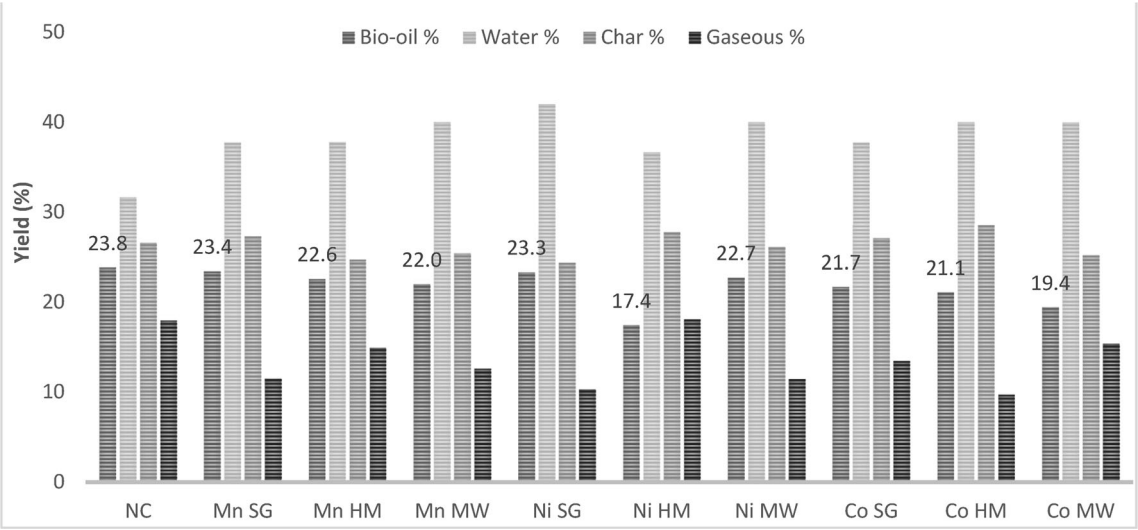

Fig. 8 Product yield distribution of non-catalytic and catalytic date stone pyrolysis experiments

a decrease in the quantity, nevertheless also an improvement in the quality of the bio-oil for formation of more H_2O. Perovskite-type catalysts increased the yield of water by promoting the extension of dehydration reactions of oxygenated compounds during pyrolysis.

3.3.1 Catalyst effectiveness

Bio-oil selectivity is an important parameter indicating the effectiveness of converting a certain biomass into various hydrocarbons besides oxygenated compounds [4]. In order to analyse the effectiveness of pyrolysis reactions, conversion in terms of activity and bio-oil selectivity are evaluated for each test. The desired product in the calculation of selectivity and yield is bio-oil; undesired products are char, water and gas. As a result of pyrolysis, the catalyst which has the highest yield of desired liquid product is the most effective catalyst. The activity calculations of the catalysts are given in Table 2.

Table 2 The performance of the perovskite catalysts in terms of activity and selectivity

Catalyst	Y_i (% ağ.)	S_i	$K_{effectiveness}$
NC	23.80	0.31	–
Co SG	21.71	0.28	6.02
Co HM	21.11	0.27	5.69
Co MW	19.43	0.24	4.69
Mn SG	23.45	0.31	7.18
Mn HM	22.57	0.29	6.58
Mn MW	22.00	0.28	6.20
Ni SG	23.33	0.30	7.10
Ni HM	17.44	0.21	3.69
Ni MW	22.73	0.29	6.66

According to the results, the perovskite effectiveness is strongly affected by the preparation method rather than B-site metal type. Among the synthesized perovskites, sol-gel-prepared $LaMnO_3$ provided highest bio-oil yield. When the effect of the preparation method was considered, it was found out that hydrothermal synthesis followed sol-gel method. On B-side metal effect, nickel was followed by manganese. Cobalt was the least active catalyst among the used ones.

3.3.2 Catalyst reusability

A catalyst plays a vital role in heterogeneous chemical reactions. On the other hand, catalysts have a limited life time. Catalysts are known to be deactivated by a long duration of reaction, thermal degradation, poisoning and sintering. Hence, the reuse technology of spent catalysts is a worth contemplation before becoming useless waste [44, 45]. In this study, reusability experiments were carried out at optimum number of tests according to the literature [46, 47]. The experiments were conducted in the presence of $LaMnO_3$, which is the most active catalysts in date stone pyrolysis, with N_2 flow rate of 100 cm^3/min, 100 °C/min heating rate, 15-min residence time and 520 °C pyrolysis temperature. The catalyst is placed in a layer of steel wool between the reactant and the biomass, thereby providing pyrolysis vapours over the catalyst. The results obtained from pyrolysis experiments and the product distributions are given in Fig. 9. In general, bio-oil and gaseous product yields improved, while water and char product yields declined. This can be related to by the fact that the vapours released during the pyrolysis pass through the catalyst, the more efficient decomposition and the volatile sieve occur. In the second use compared with the first use, the liquid and solid products decreased while the water and gaseous product yield increased. In the third, the fourth and the fifth uses of the catalyst, the productivity of the liquid, water and

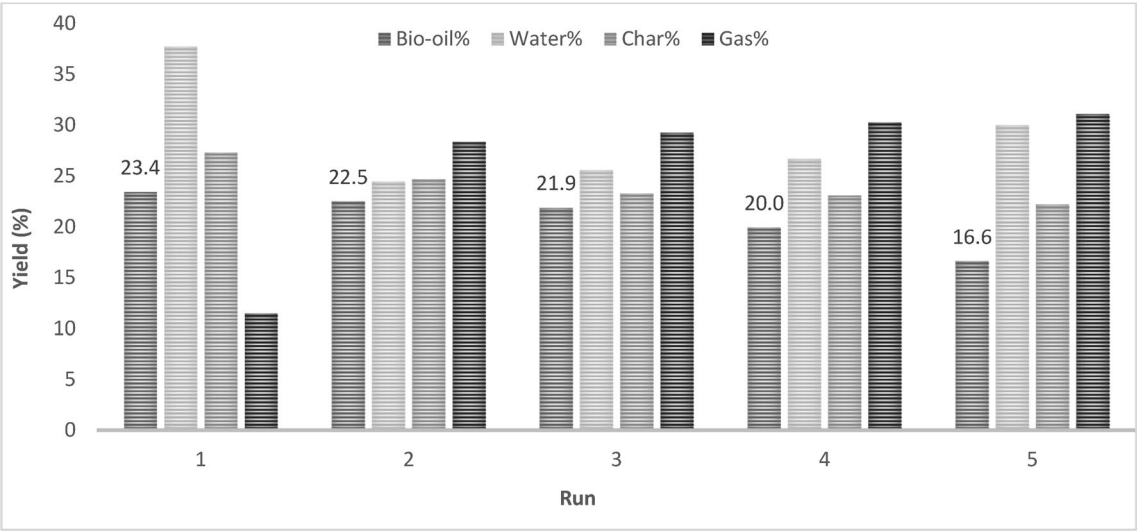

Fig. 9 Five-run recycling test of sol-gel-prepared $LaMnO_3$ for pyrolysis of DS

solid products was decreased while the gas product yield was raised. Similar results were accepted by different researchers in the literature [48]. In a review published in 2001 by Sutton et al., a number of nickel-containing catalysts have been reported to be effective in the gasification of biomass and have been used effectively for this purpose. The reusability of the Mg/Al-MCM-41 catalyst synthesized was investigated by Karnjanakom et al. in their work in 2017 and the correlated amount of total hydrocarbon decreases with the amount of coke build-up on the active surface of the catalyst causing the catalyst to lose its activity during the reaction [47].

3.4 Bio-oil characterization

3.4.1 Elemental analysis of bio-oils

One of the important parameters about bio-oil is the elemental composition. Elemental composition of bio-oils, O/C and H/C molar ratios and higher heating values were evaluated under thermal pyrolysis, and catalytic pyrolysis bio-oils are given in Table 3. In catalytic pyrolysis, optimum catalyst was selected as $LaMnO_3$ catalyst arranged by sol-gel method used according to bio-oil yield. The carbon content of catalytic pyrolysis bio-oil is superior to non-catalytic one. The hydrogen content of bio-oil improved with existence of perovskite. For the H/C ratios of bio-oils, catalytic pyrolysis gave higher ratio than non-catalytic pyrolysis rising from 1.51 to 1.64. Additionally, the energy density of non-catalytic bio-oil was enhanced as pointed out by the HHVs of the bio-oils.

3.4.2 Functional groups of bio-oils

The vibrational spectrum of a molecule is considered as a unique physical property and characteristic of a molecule. FT-IR analysis gives an infrared spectrum which is very useful as a fingerprint for the identification of functional groups of unidentified compounds by producing characteristic and reproducible absorption. This valuable contribution aids to show whether the molecule is linear or branched chain aliphatic or aromatic compound [49]. FT-IR outcomes of bio-oils attained under catalytic and non-catalytic conditions are summarized in Fig. 10. FT-IR results confirmed that bio-oils

Table 3 Elemental composition of bio-oils, O/C and H/C molar ratios and higher heating values (HHV) evaluated under thermal pyrolysis and catalytic pyrolysis bio-oils

	Non-catalytic bio-oil	Sol-gel-prepared $LaMnO_3$ used bio-oil
C	60.92	64.51
H	7.75	8.92
N	6.48	0.10
O*	24.85	26.47
H/C	1.51	1.64
O/C	0.30	0.30
Molar formula	$CH_{1.52}N_{0.09}O_{0.30}$	$CH_{1.65}N_{0.01}O_{0.30}$
HHV (MJ/kg)	27.31	29.92

* Calculated from difference

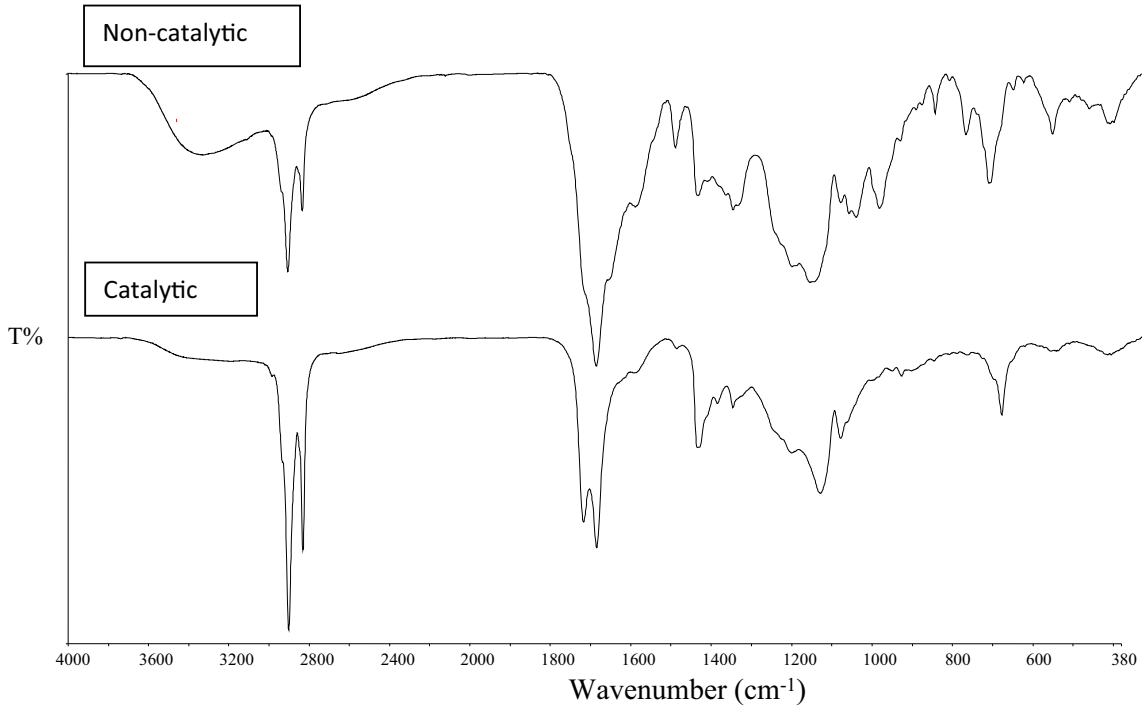

Fig. 10 FT-IR spectrum of non-catalytic and catalytic bio-oil

restrained similar functional groups with a variation in intensity. The O-H stretching vibration band at 3335 cm^{-1} is significantly reduced and virtually missed in perovskite used bio-oil spectrum. The C-H stretching vibrations between 2900 and 2800 cm^{-1} and C-H deformation vibrations between 1450 and 1350 cm^{-1} showed the existence of alkanes. These peak intensities increased in catalytic bio-oil. Moreover, the location of bending vibration of C-H groups at 1375 cm^{-1} delivered additional indication of the methyl groups. The peaks between 1675 and 1575 cm^{-1} indicated C-C stretching vibrations which indicated the presence of aromatics and alkenes. These peaks are more evident for non-catalytic pyrolysis. The C-O stretching vibrations between 1740 and 1680 cm^{-1} represented the presence of aldehydes or ketones. The intensities of these two peaks of non-catalytic bio-oil are higher than catalytic one. The existence of both C-O and O-H stretching vibrations also proved the presence of carboxylic acids and derivatives, so non-catalytic bio-oil was found richer in terms of these compounds compared with perovskite catalyst used bio-oil. The area between 800 and 650 cm^{-1} contained various bands related with the aromatic, out of plane C-H bending. The high intensity of these bands of non-catalytic bio-oil indicates that the aromatic hydrogen was found in aromatic rings with high degree of substitution.

3.4.3 ^{1}H-NMR-based structural analyses

^{1}H-NMR spectra were obtained for non-catalytic and optimum catalyst ($LaMnO_3$ prepared by sol-gel) used bio-oils and the results are set in Table 4. The region of the spectra, from 0 to 1.5 ppm, signifying aliphatic protons was the more settled for all bio-oils (>50% of all protons) representing great

Table 4 Results of ^{1}H-NMR of bio-oils in terms of percentage hydrogen total

Proton assignment	Chemical shift region (ppm)	Non-catalytic bio-oil	Sol-gel-prepared $LaMnO_3$ used bio-oil
CH_3 γ or further from an aromatic ring	0.5–1.0	10.23	11.33
β -CH_3, CH_2 and CH γ or further from an aromatic ring	1.0–1.5	45.00	42.72
CH_2 and CH β to an aromatic ring (naphthenic)	1.5–2	8.70	6.15
CH_3. CH_2 and CH to an aromatic ring	2.0–3.0	13.25	10.24
Ring-join methylene (Ar-CH_2-Ar)	3.0–4.5	4.23	7.70
Phenolic (OH) or olefinic proton	4.5–6.0	12.66	16.26
Aromatic	6.0–9.0	5.93	5.60
Aldehydes (R-CHO) and/or carboxylic acids (R-COOH)	9.0–12.0	–	–

aliphatic content. Catalytic bio-oil had less pronounced production of alkanes compared with non-catalytic. The 1.5–3.0 ppm region signifies protons on aliphatic carbon atoms to be bonded to a C=C double bond (aromatic or olefinic) or are two bonds away from a heteroatom. Non-catalytic bio-oil contains greater levels of protons in this area. In the 3.0–4.5 ppm spectrum, it represents protons on carbon atoms next to an aliphatic alcohol or ether or a methylene group that links two aromatic rings. The attendance of these oxygenated compounds (4.23% in non-catalytic bio-oil), qualified an increment (7.70%) as a consequence of the catalyst. The region between 4.5 and 6.0 ppm shows aromatic ether protons and many of the hydrogen atoms of carbohydrate-like molecules. These sorts of molecules are in higher amount in especially catalytic bio-oil which is consistent with the O content. The aromatic region which falls between 6.0 to 9.0 ppm has similar amounts of the protons in the bio-oils. The aromaticity of the bio-oil of non-catalytic pyrolysis was slightly higher than the catalytic bio-oil. Then, aldehydes and carboxylic acids (9.0 to 12.0 ppm) were not identified in any of bio-oils. Overall, the ^{1}H-NMR analysis demonstrated that aliphatic protons are most predominant for bio-oils derived from date seed in both catalytic and non-catalytic conditions. While the perovskite catalyst decreased the aliphatic compounds, it increased the total oxygenated compounds in terms of phenolics in comparison with non-catalytic bio-oil.

4 Future perspectives

This study provides both date seed yields and bio-oil characterization result in lab scale which can be utilized further for adapting large scales. The data from this work can be imported in order to evaluate in a techno-economic model including investment and operating cost of a date seed catalytic pyrolysis process similar to the study reported by Vasalos et al. (2016). Their study focused on the economic assessment of catalytic bio-oil production from processing biomass as well as establishing a detailed design and cost models via ASPEN. According to their results, low-cost biomass and inexpensive catalysts are the vital factors deciding the future of catalytic pyrolysis process [50]. Their study opens a new window in order to lay out the benefits of lab-scale pyrolytic runs in favour of carrying the experiments to industrial scale besides its environmental benefits. On the other hand, this still needs to be investigated in depth in future work.

5 Conclusion

Date stone was used as feedstock for pyrolysis bio-oils. Its high carbon content makes it an appropriate feedstock for bio-fuel production. When the SEM images were examined, the date stone has indented protruding particles and an almost non-porous structure. Among the synthesis methods, sol-gel was found to be more effective when pure phase is considered. Manganese-based perovskites has higher S_{BET} values compared with Ni and Co ones. The pores in structures of perovskites were well and not uniformly distributed. Wide pore size distribution for the whole samples was observed, ranging from 5 to 80 nm. In the presence of a perovskite catalyst in pyrolysis, bio-oil, char and gas yields decreased. The decline in bio-oil yield in terms of perovskite used could be attributed to competing reaction, most likely conversion reactions occurring during pyrolysis. This suggests that the additional conversion of bio-oils over the catalysts resulted in a decrease of bio-oil yield. Among the catalysts, $LaMnO_3$ prepared by sol-gel is the most effective catalyst. According to the results, the perovskite effectiveness is strongly affected by the preparation method rather than B-site metal type. The results showed that using perovskite can be as a potential way of producing adequate amounts and the quality of bio-oil needs to be performed as in future researches.

Availability of data and material The data that support the findings of this study are available from the corresponding author, NÖ, upon reasonable request.

Compliance with ethical standards

Conflict of interest The authors declare that they have no conflict of interest.

Code availability Not applicable.

References

1. Murata K, Kreethawate L, Larpkiattaworn S, Inaba M (2016) Evaluation of Ni-based catalysts for the catalytic fast pyrolysis of jatropha residues. J Anal Appl Pyrolysis. https://doi.org/10.1016/j.jaap.2016.02.014
2. Sepehri A, Sarrafzadeh MH (2018) Effect of nitrifiers community on fouling mitigation and nitrification efficiency in a membrane bioreactor. Chem Eng Process Process Intensif. https://doi.org/10.1016/j.cep.2018.04.006
3. Whyte HE, Loubar K, Awad S, Tazerout M (2015) Pyrolytic oil production by catalytic pyrolysis of refuse-derived fuels: investigation of low cost catalysts. Fuel Process Technol. https://doi.org/10.1016/j.fuproc.2015.08.022
4. Ozbay N, Yargic AS, Yarbay Sahin RZ (2018) Tailoring cu/Al2O3 catalysts for the catalytic pyrolysis of tomato waste. J Energy Inst. https://doi.org/10.1016/j.joei.2017.01.010
5. Kabir G, Hameed BH (2017) Recent progress on catalytic pyrolysis of lignocellulosic biomass to high-grade bio-oil and bio-chemicals. Renew Sust Energ Rev. https://doi.org/10.1016/j.rser.2016.12.001
6. Hernando H, Fermoso J, Ochoa-Hernández C et al (2018) Performance of MCM-22 zeolite for the catalytic fast-pyrolysis of acid-washed wheat straw. Catal Today. https://doi.org/10.1016/j.cattod.2017.09.043

7. Özbay N, Yargıç AŞ, Yarbay Şahin RZ, Yaman E (2018) Research on the pyrolysis characteristics of tomato waste with Fe–Al 2 O 3 catalyst. Exergetic, Energ Environ Dimens:815–828. https://doi.org/10.1016/B978-0-12-813734-5.00046-9
8. Blasco J, Sánchez MC, Pérez-Cacho J et al (2002) Synthesis and structural study of LaNi1-xMnxO3+δ perovskites. J Phys Chem Solids. https://doi.org/10.1016/S0022-3697(01)00228-1
9. Jeon Y, Lee C, Rhee J et al (2017) Autothermal reforming of heavy-hydrocarbon fuels by morphology controlled perovskite catalysts using carbon templates. Fuel. https://doi.org/10.1016/j.fuel.2016.09.065
10. Ozbay N, Yargic A, Sahin R et al (2019) Valorization of banana peel waste via in-situ catalytic pyrolysis using Al-modified SBA-15. Elsevier 140:633–646. https://doi.org/10.1016/j.renene.2019.03.071
11. Yang Y, Lv G, Deng L et al (2017) Renewable aromatic production through hydrodeoxygenation of model bio-oil over mesoporous Ni/SBA-15 and co/SBA-15. Microporous Mesoporous Mater. https://doi.org/10.1016/j.micromeso.2017.05.022
12. Kim YM, Jae J, Lee HW et al (2016) Ex-situ catalytic pyrolysis of citrus fruit peels over mesoporous MFI and Al-MCM-41. Energy Convers Manag. https://doi.org/10.1016/j.enconman.2016.02.065
13. Grieco EM, Gervasio C, Baldi G (2013) Lanthanum-chromium-nickel perovskites for the catalytic cracking of tar model compounds. Fuel. https://doi.org/10.1016/j.fuel.2012.09.017
14. Ammendola P, Lisi L, Piriou B, Ruoppolo G (2009) Rh-perovskite catalysts for conversion of tar from biomass pyrolysis. Chem Eng J. https://doi.org/10.1016/j.cej.2009.04.010
15. Sun X, Wang S, Wang Z et al (2008) Anode performance of LST–xCeO2 for solid oxide fuel cells. J Power Sources 183:114–117. https://doi.org/10.1016/J.JPOWSOUR.2008.05.007
16. Hameed BH, Salman JM, Ahmad AL (2009) Adsorption isotherm and kinetic modeling of 2,4-D pesticide on activated carbon derived from date stones. J Hazard Mater. https://doi.org/10.1016/j.jhazmat.2008.06.069
17. Al-Omari SAB (2009) Evaluation of the biomass "date stones" as a fuel in furnaces: a comparison with coal combustion. Int Commun Heat Mass Transf. https://doi.org/10.1016/j.icheatmasstransfer.2009.06.016
18. Bouchelta C, Medjram MS, Bertrand O, Bellat JP (2008) Preparation and characterization of activated carbon from date stones by physical activation with steam. J Anal Appl Pyrolysis. https://doi.org/10.1016/j.jaap.2007.12.009
19. Taallah B, Guettala A (2016) The mechanical and physical properties of compressed earth block stabilized with lime and filled with untreated and alkali-treated date palm fibers. Constr Build Mater. https://doi.org/10.1016/j.conbuildmat.2015.12.007
20. Sekirifa ML, Hadj-Mahammed M, Pallier S et al (2013) Preparation and characterization of an activated carbon from a date stones variety by physical activation with carbon dioxide. J Anal Appl Pyrolysis. https://doi.org/10.1016/j.jaap.2012.10.007
21. Ahmed MJ (2016) Preparation of activated carbons from date (Phoenix dactylifera L.) palm stones and application for wastewater treatments: review. Process Saf Environ Prot
22. Khelaifia FZ, Hazourli S, Nouacer S et al (2016) Valorization of raw biomaterial waste-date stones-for Cr (VI) adsorption in aqueous solution: thermodynamics, kinetics and regeneration studies. Int Biodeterior Biodegrad. https://doi.org/10.1016/j.ibiod.2016.06.002
23. Abbas AF, Ahmed MJ (2016) Mesoporous activated carbon from date stones (Phoenix dactylifera L.) by one-step microwave assisted K2CO3 pyrolysis. J Water Process Eng. https://doi.org/10.1016/j.jwpe.2016.01.004
24. Danish M, Hashim R, Ibrahim MNM, Sulaiman O (2014) Optimized preparation for large surface area activated carbon from date (Phoenix dactylifera L.) stone biomass. Biomass Bioenergy. https://doi.org/10.1016/j.biombioe.2013.12.008
25. Belhamdi B, Merzougui Z, Trari M, Addoun A (2016) A kinetic, equilibrium and thermodynamic study of L-phenylalanine adsorption using activated carbon based on agricultural waste (date stones). J Appl Res Technol. https://doi.org/10.1016/j.jart.2016.08.004
26. Danish M, Khanday WA, Hashim R et al (2017) Application of optimized large surface area date stone (Phoenix dactylifera) activated carbon for rhodamin B removal from aqueous solution: Box-Behnken design approach. Ecotoxicol Environ Saf. https://doi.org/10.1016/j.ecoenv.2017.02.001
27. Al-Badri HT, Lafta SJ, Barbooti MM, Al-Sammerrai DA (1989) The thermogravimetry and pyrolysis of date stones. Thermochim Acta. https://doi.org/10.1016/0040-6031(89)85183-4
28. Yarbay RZ, Figen HE, Baykara SZ (2012) Effects of cobalt and nickel substitution on physical properties of perovskite type oxides prepared by the sol-gel citrate method. Acta Phys Pol A 121:44–46. https://doi.org/10.12693/APhysPolA.121.44
29. Guldal NO, Figen HE, Baykara SZ (2017) Production of hydrogen from hydrogen sulfide with perovskite type catalysts: LaMO3. Chem Eng J. https://doi.org/10.1016/j.cej.2016.11.057
30. Zhang L, Zhang Y, Dai H et al (2010) Hydrothermal synthesis and catalytic performance of single-crystalline La2-xSrxCuO4 for methane oxidation. Catal Today. https://doi.org/10.1016/j.cattod.2010.02.059
31. Ifrah S, Kaddouri A, Gelin P, Leonard D (2007) Conventional hydrothermal process versus microwave-assisted hydrothermal synthesis of La1-xAgxMnO3+δ (x = 0, 0.2) perovskites used in methane combustion. Comptes Rendus Chim. https://doi.org/10.1016/j.crci.2007.08.002
32. Adjaye JD, Bakhshi NN (1995) Production of hydrocarbons by catalytic upgrading of a fast pyrolysis bio-oil. Part II: Comparative catalyst performance and reaction pathways. Fuel Process Technol. https://doi.org/10.1016/0378-3820(95)00040-E
33. Maisano S, Urbani F, Mondello N, Chiodo V (2017) Catalytic pyrolysis of Mediterranean Sea plant for bio-oil production. Int J Hydrog Energy. https://doi.org/10.1016/j.ijhydene.2017.07.124
34. Özçimen D, Ersoy-Meriçboyu A (2010) Characterization of biochar and bio-oil samples obtained from carbonization of various biomass materials. Renew Energy. https://doi.org/10.1016/j.renene.2009.11.042
35. Soleymani M, Moheb A, Joudaki E (2009) High surface area nanosized La0.6Ca0.4 MnO3 perovskite powder prepared by low temperature pyrolysis of a modified citrate gel. Cent Eur J Chem. https://doi.org/10.2478/s11532-009-0083-2
36. Campagnoli E, Tavares A, Fabbrini L et al (2005) Effect of preparation method on activity and stability of LaMnO 3 and LaCoO 3 catalysts for the flameless combustion of methane. Appl Catal B Environ. https://doi.org/10.1016/j.apcatb.2004.07.010
37. Vaz T, Salker AV (2007) Preparation, characterization and catalytic CO oxidation studies on LaNi1-xCoxO3 system. Mater Sci Eng B Solid-State Mater Adv Technol. https://doi.org/10.1016/j.mseb.2007.07.027
38. Makshina EV, Zhilinskaya EA, Aboukais A, Romanovskii BV (2007) Valence and coordination state of cobalt atoms in bulk and deposited lanthanum cobaltates. Mosc Univ Chem Bull. https://doi.org/10.3103/S0027131407010026
39. Le Dréau L (2011) Phase transitions and oxygen ordering in La2CoO4+δ and (T, T')-La2CuO4: single crystal growth and structural studies using synchrotron and neutron diffraction methods. PhD Dissertation. Université Rennes. https://tel.archives-ouvertes.fr/tel-00634848
40. Guo J, Lou H, Zhu Y, Zheng X (2003) La-based perovskite precursors preparation and its catalytic activity for CO2 reforming of CH4. Mater Lett. https://doi.org/10.1016/S0167-577X(03)00341-0

41. Kirchnerova J, Klvana D (1999) Synthesis and characterization of perovskite catalysts. Solid State Ionics. https://doi.org/10.1016/S0167-2738(99)00102-2
42. Fidalgo A, Ciriminna R, Lopes L et al (2013) The sol-gel entrapment of noble metals in hybrid silicas: a molecular insight. Chem Cent J. https://doi.org/10.1186/1752-153X-7-161
43. Keav S, Matam SK, Ferri D, Weidenkaff A (2014) Structured perovskite-based catalysts and their application as three-way catalytic converters-a review. Catalysts. https://doi.org/10.3390/catal4030226
44. Lesmana D, Wu HS (2015) Pyrolysis of waste oil in the presence of a spent catalyst. J Environ Chem Eng. https://doi.org/10.1016/j.jece.2015.09.019
45. Song X, Wu Y, Cai F et al (2017) High-efficiency and low-cost li/ZnO catalysts for synthesis of glycerol carbonate from glycerol transesterification: the role of li and ZnO interaction. Appl Catal A Gen. https://doi.org/10.1016/j.apcata.2016.12.019
46. Karagöz S, Kawakami T, Kako A et al (2016) Single shot pyrolysis and on-line conversion of lignocellulosic biomass with HZSM-5 catalyst using tandem micro-reactor-GC-MS. RSC Adv. https://doi.org/10.1039/c6ra04225b
47. Karnjanakom S, Suriya-umporn T, Bayu A et al (2017) High selectivity and stability of mg-doped Al-MCM-41 for in-situ catalytic upgrading fast pyrolysis bio-oil. Energy Convers Manag. https://doi.org/10.1016/j.enconman.2017.03.049
48. Sutton D, Kelleher B, Ross JRH (2001) Review of literature on catalysts for biomass gasification. Fuel Process Technol. https://doi.org/10.1016/S0378-3820(01)00208-9
49. Shadangi KP, Mohanty K (2014) Thermal and catalytic pyrolysis of Karanja seed to produce liquid fuel. Fuel. https://doi.org/10.1016/j.fuel.2013.07.053
50. Vasalos IA, Lappas AA, Kopalidou EP, Kalogiannis KG (2016) Biomass catalytic pyrolysis: process design and economic analysis. Wiley Interdiscip Rev Energy Environ. https://doi.org/10.1002/wene.192